Atom Indonesia

Journal homepage: https://atomindonesia.brin.go.id

Modeling of ^{137}Cs Dispersion in the Atlantic Ocean at Ahanta West Coast: A Hypothetical Candidate Site for Ghana's First Nuclear Power Plant

Y. A. Aggrey[1]*, M. Amo-Boateng[1], D. O. Kpeglo[2], M. Muslim[3], A. T. Prasteyo[3]

[1]*Department of Civil and Environmental Engineering, University of Energy and Natural Resources, Sunyani 214, Ghana*
[2]*Radiation Protection Institute, Ghana Atomic Energy Commission, Legon LG80, Ghana*
[3]*Department of Oceanography, Diponegoro University, Semarang 50275, Indonesia*

ARTICLE INFO

Article history:
Received 24 June 2023
Received in revised form 28 December 2023
Accepted 31 December 2023

Keywords:
Ahanta west
Nuclear power plant
^{137}Cs
Rainy season
Dry season

ABSTRACT

The government of Ghana has the intention of adding nuclear to its energy mix. Due to water availability for cooling, the coastal areas will be the right place for siting a nuclear power plant. This study was carried out to assess the distribution of ^{137}Cs should liquid radioactive waste be released into coastal waters because of a non-routine event. The distribution was studied for the first month after the release. In the first week following the release, ^{137}Cs was distributed within 16 km of the Ahanta West coastal waters with a concentration of about 9.1 Bq. L^{-1}. On the seventh day, the distribution reached the entire coast of the Nzema East with a lower concentration with the bulk of the concentration still in the Ahanta waters. The ^{137}Cs continued to spread into the eastern coast until the thirty-first day with a concentration of less than 1 Bq. L^{-1}. This study provides useful data for future monitoring along the coast.

INTRODUCTION

During the last 60 years, human activity has resulted in varying degrees of contamination of the world's oceans with anthropogenic radionuclides. The main contribution to anthropogenic marine radioactivity is from global fallout from nuclear tests performed in the atmosphere, particularly in the 1950s and 1960s [1]. While humans are constantly exposed to external radiation from cosmic and terrestrial radiation, radionuclides in the sea typically may contribute more to internal exposure via ingestion. As of 2000, the total inventories of three of the most studied anthropogenic radionuclides in the world's oceans were 200 PBq, 350 PBq, and 10 PBq for ^{90}Sr, ^{137}Cs, and ^{239,240}Pu respectively [2].

Among these artificial radionuclides is ^{137}Cs, which is a by-product of the nuclear fission of uranium-235 in nuclear reactors and nuclear weapons. ^{137}Cs is released into the environment from artificial sources, with global nuclear tests being the main contributor as well as nuclear accidents [1]. The conservative nature of ^{137}Cs in seawater allows its distribution to be strongly influenced by seawater mass movement [3]. ^{137}Cs is transported within the ocean by advection and diffusion, with their activity levels reduced due to radioactive decay [4]. The concentration of ^{137}Cs in seawater has a significant impact on its concentration in marine organisms. As soon as ^{137}Cs enters the marine environment, it dissolves in the water column and is carried by ocean currents, which has the potential to contaminate a wide area.

Furthermore, ^{137}Cs can contaminate sediments by attaching itself to particles and settling on the seafloor. Marine life can absorb ^{137}Cs directly from the ocean or by consuming contaminated food. Predators can collect larger amounts of ^{137}Cs than their prey because ^{137}Cs can biomagnify up the food chain [4]. Exposure to high levels of ^{137}Cs can cause physiological stress and damage to marine organisms, potentially leading to reduced growth, impaired reproduction, and mortality. Contaminated fish and shellfish pose great risks to human health if

*Corresponding author.
E-mail address: yaaggrey@gmail.com
DOI: https://doi.org/10.55981/aij.2024.1344

consumed. Long-term exposure to ^{137}Cs raises the risk of developing cancer, especially bone and soft tissue malignancies.

During the normal operation of a nuclear power plant, controlled releases of liquid radioactive wastes into the marine environment can occur in regulated concentrations and quantities. However, in emergency or non-routine scenarios, releases may occur above regulated limits. For example, numerical modeling was applied to simulate the transport of ^{137}Cs which will be released by the Japanese government into the ocean due to unavailable storage space [5]. The water still includes radionuclides with long half-lives and may potentially contaminate marine habitats and pose a concern to human health, even though it is typically processed by an Advanced Liquid Processing System (ALPS) [6].

The government of Ghana has indicated adding nuclear power to its energy mix. The National Energy Transition framework's aim is to integrate nuclear power into the national electricity generation mix for long-term supply security as well as to help in addressing climate change and reducing air pollution [7]. The first nuclear power plant in Ghana is expected to be built and put into service in 2024 and 2030, respectively, according to the nuclear power program's roadmap. The initiative is currently in Phase 2, where construction-related preparatory work is ongoing. These include the selection of vendors, creation of TORs for site assessments, development of human resources, and stakeholder engagements. Most nuclear power plants in the world are sited along the coast due to the availability of water for cooling. As nuclear power plants use seawater for cooling, it must be ensured that the marine environment around them is protected from radioactive releases.

Lots of marine dispersion model studies for nuclear power plants have been conducted by many researchers all over the world. Aside from biological factors and chemical reactions, the ocean current is a dominant factor in the determination of ^{137}Cs concentrations in seawater [8]. Very limited research has been carried out on the dispersion of radionuclides in Ghana's marine waters as well as information concerning the radioactivity in the marine environment of West Africa which includes Ghana is very scarce. Ahanta West is a coastal area in Ghana and has been taken as a hypothetical site for the nuclear power plant in this study. There will be a need to know how radionuclides will disperse in the coastal waters around the plant should there be a non-routine release into the marine environment.

The aim of this study is to model the distribution of ^{137}Cs in seawater following an unplanned release from a nuclear power plant at a hypothetical site in Ahanta West to determine how far it will spread. This simulation can help serve as a reference for taking precautions should such an event occur.

METHODOLOGY

Design model

The candidate site for the hypothetical nuclear power plant considered in this study was the Ahanta West District in the Western Region of Ghana (Fig. 1). The government has yet to decide on the type of reactor; it was assumed to be a Pressurized Water Reactor (PWR), AP1000, due to its common usage worldwide. The AP1000, developed by Westinghouse with a net electrical output of about 1,117 MWe, is notable for its safety features, including passive safety systems.

This study simulated a non-routine event resulting in the release of ^{137}Cs during the two different seasons, rainy and dry seasons, in Ghana. The distribution model was built by using the Eulerian model, Delft3d flow module. The flow module is a multi-dimensional (2D or 3D) hydrodynamic (and transport) simulation programme that calculates non-steady flow and transport phenomena resulting from tidal and meteorological forcing on the curvilinear, boundary-fitted grid or spherical coordinates. Due to the shallow ocean depth of about 200 m in the study area, 2D was applied.

Fig. 1. The study area.

Table 1. ^{137}Cs discharge scenarios.

Scenario	Volume (m^3)	Duration (h)	Discharge rate ($m^3.s^{-1}$)	Concentration ($Bq.m^{-3}$)
Rainy season Dry season	100	10	0.00278	2. 10^5

The ^{137}Cs release scenarios are presented in Table 1.1 GWe PWRs produce low-level radioactive waste of 250 m^3 per year [9], while the limit for ^{137}Cs radionuclide activity that is allowed to be discharged into the ocean is about $5x10^7$ Bq [10]. The concentration of $_{137}$Cs, $2x10_5$ Bq.m$_{-3}$, released in the non-routine scenario was decided by dividing the ^{137}Cs activity limit, $5x10^7$ Bq, by annual waste volume, 250 m^3. Therefore, the release rate can be controlled to be within the limit. For the waste discharge value ($0.00278m^3.s^{-1}$), it was assumed the waste is disposed of through a canal towards the coastal sea. This value therefore adjusted to the discharge of small rivers. IAEA recorded some estimates of river discharge for river's average width and depth. Dumping duration of 10 hrs was obtained by dividing the waste volume (100 m^3) by the waste discharge, $0.00278m^3.s^{-1}$ and converting the seconds to hours. The volume of 100 m^3 used based on an assumption made from a similar study. Both volume and discharge rate were determined based on the highest ^{137}Cs release in previous research [11]. This way assures a conservative approach to safety and radiation protection of the environment.

Data source and simulated procedure

All data with their filenames as input data for the Delft3D 4 suite hydrodynamical model are presented in Table 2. The required data for this research were bathymetry, observed tide, surface wind, and bottom sediment. GEBCO_2020 bathymetry data (http://www.gebco.net) delivered by the British Oceanographic Centre was processed through ArcGIS 10.6 to transform its format into xyz. The shoreline shapefiles for the study area were obtained from Ghana Open Data Initiative (data.gov.gh). The boundary model at Delft3D is usually called Land Boundary which was constructed based on model design and shoreline (Fig. 1).

Table 2. Required data used for model.

No	Data	Definition
1.	Land Boundary	Shoreline, island, and boundary in the model area
2.	Grid	Mesh of model
3.	Dry Point	Varied grids which located in the island
4.	Depth	Water bathymetric
5.	Boundary	The entire open boundary (water to water)
6.	Water level	Tide variable by type time-series
7.	Wind	Included of speed and direction
8.	Monitoring	Defined grids where validated data was observed

Furthermore, land boundary data was used as a reference in the process of making grids and islands within the scope of the model area in the RGFGRID Delft3D module. Time series tidal data was obtained using WXTide32 software. The reference station used was Takoradi station in the Western Region of Ghana and the closest to the study area. The text tide output type used was incremental, with a tide step of 60 minutes and a length of 31 days. The hourly tide data was used in this study with a period adjusting to the model period. Furthermore, this hourly tide in time series was entered into the open boundary through the Delft3d flow module. Surface wind speed and direction, including u and v components, were obtained from the Ghana Meteorological Agency. The *u* and *v* wind components are then converted to obtain the wind speed and direction [12].

Model validation

Validating data was quite important to analyze whether the model had illustrated sufficiently the real conditions in general or did not describe them at all. This study only validated the result of the hydrodynamic model, such as the tidal model and ocean current model. The dynamic of ^{137}Cs was not validated because this study only examined the potential for ^{137}Cs distribution from a nuclear power plant that has not been built. The tidal model was validated with tidal data from (WXTide32 software), while the ocean current model was validated with the data Global_Analysis_Forecast_Phy_001_024 (https://marine.copernicus.eu/) in a resolution of 0.083 degrees created by Marine Copernicus. Root Mean Square Error (RMSE) approach was used to validate both model data [13,14], which are expressed in Eq. 1.

$$\mathrm{RMSE} = \sqrt{\frac{\sum_{i=1}^{n}(O_i - S_i)^2}{n}} \quad (1)$$

Where O_i and S_i are the value of observed and simulated data, respectively. The amount of data was illustrated as "n". The model incorporates various parameters with corresponding values as shown in Table 3.

Table 3. Values used in the model.

Parameter	Unit	Value	Reference
Gravity (default)	$m.s^{-1}$	9.81	[15]
Water density	$kg.m^{-3}$	1025	[15]
Air density (default)	$kg.m^{-3}$	1	[15]
Roughness	*White - Colebook*	U = 0.05 V = 0.05	[15]
Viscosity (Default)	$m^2.s^{-1}$	1	[15]
Horizontal Diffusion of ^{137}Cs	$m^2.s^{-1}$	50	[16]
Distribution coefficient of ^{137}Cs	$L.kg^{-1}$	4000	[17]

RESULTS AND DISCUSSION

Verification model

Verifying surface elevation and the velocities (X and Y components) together is crucial for a comprehensive understanding of water movement and dispersion dynamics. Surface elevation is closely linked to tidal movements, storm surges, and other phenomena. These changes in elevation can impact current velocities. The model and observed data are in close agreement for most of the duration, with only minor discrepancies. This implies that the model accurately captures the periodic changes in surface elevation, which is vital for predicting how ^{137}Cs might move vertically in the water column. Velocities (both X and Y components) represent horizontal water movement. The X component has some deviations between the model and observations, especially in the magnitude of velocity peaks. However, the model seems to capture the general pattern accurately. Similar to the X component, there's a clear periodicity, and while there are discrepancies, the overall pattern between the model and observations is closely aligned. The comparisons of model and observation data are illustrated in Figs. 2 and 3.

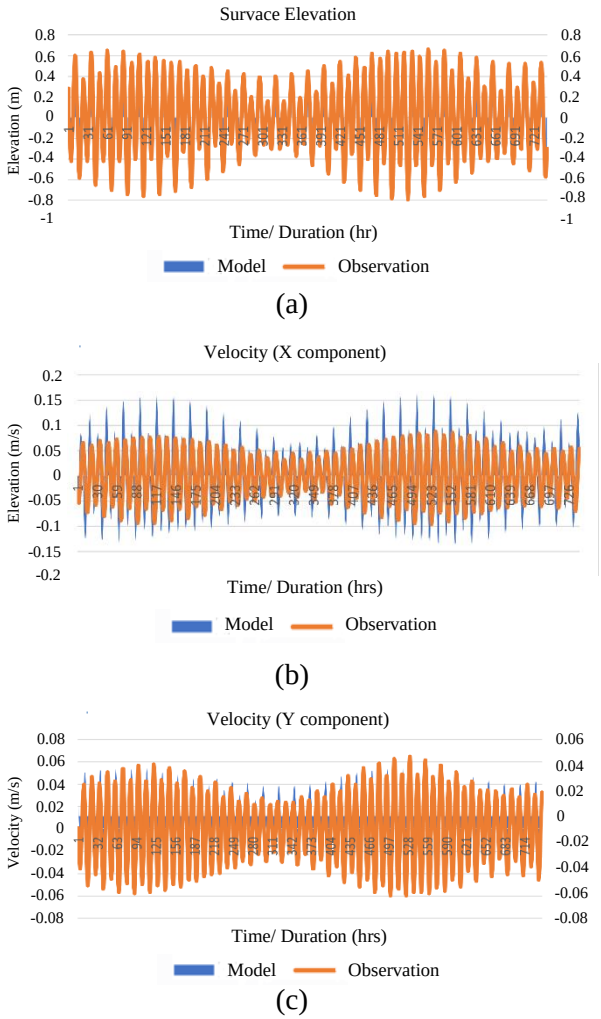

Fig. 2. Verification model for; (a) surface elevation; (b) X- component velocity; (c) Y-component velocity during rainy season.

The coastal water of Ahanta West has a mixed regular, microtidal, or semidiurnal tidal type [18], while the formzhal numbers were 0.29 (Rain Season) and 0.3 (Dry Season). It means that this coastal water sometimes experiences twice flood tide and twice ebb tides with different tidal co-range and tidal co-phase. The error values of the hydrodynamic model are presented in Table 4.

Table 4. Root Mean Relative Error of each ocean velocity model.

Parameters	RMSE Value (%)	
	Rainy Season	Dry Season
Sea level height	5.25	5.90
Ocean Velocity (x)	8.46	8.60
Ocean Velocity (y)	2.59	2.55

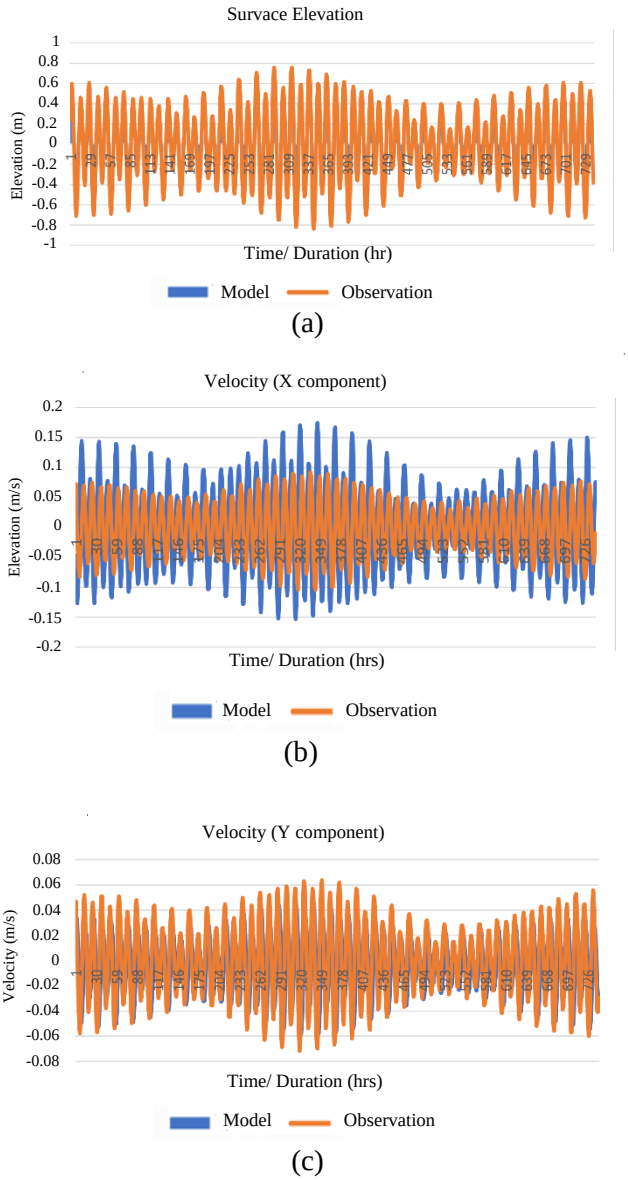

Fig. 3. Verification model for (a) surface elevation; (b) X- component velocity; (c) Y-component velocity during dry season.

Hydrodynamic model

Dry season

The distribution of sea levels at the neap tide and springtide during the dry season are presented in Figs. 4(a-d). The water level during flood neap tide is depicted in Fig. 4(a). The range of the water level is between 0.375-0.425 meters. As the water level drops, the highest levels are displayed in red, changing to orange, yellow, green, and blue. Elevated water levels in areas like Shama and Sekondi Takoradi indicate that the tide is in its flood phase. Inland, the water levels vary, with certain regions exhibiting higher levels possibly because of the flood phase. In Fig. 4(b), the water level represents the ebb neap tide and ranges from around -0.31 m to -0.21 m. The deeper water levels in the district, particularly in Sekondi Takoradi and Shama, indicate that the water is receding or ebbing away. Shallower water levels are indicated by Ellembelle. This may be the result of these places' water levels dropping during the ebb period. Smaller variations between high and low tides are the hallmark of neap tides. Figures 4(a) and 4(b), as there are not extreme variations in water levels across the districts.

Figure 4(c) shows a range of water levels from roughly 0.69 meters to 0.77 meters during the flood springtide. The coastal areas, particularly those around Sekondi and Shama, show increasing water levels that are in line with the tide's flood phase. The water level during ebb springtide as shown in Fig. 4(d) is about between -0.82 and -0.68 meters. Deeper water levels at Sekondi Takoradi and Shama indicate that during the ebb phase, water is receding from these regions. The noticeable variations in water levels along the coastal regions demonstrate the strong tidal oscillations typical of spring tides.

The tidal co-range between flood and ebb tides was around 0.7 m for the neap tide period and 1.6 m for the springtide period from the model. Flood tide is when tide is flowing in, and sea levels are rising whereas ebb tide is when tide is flowing out and sea levels are falling. The eastern coast of Ahanta West always experienced low sea levels rather than other coasts during flood tide from the model. Meanwhile, the coastal waters of Ellembelle and Nzema East experienced a rapid increase in sea level height at flood tide and a slow decrease at ebb tide.

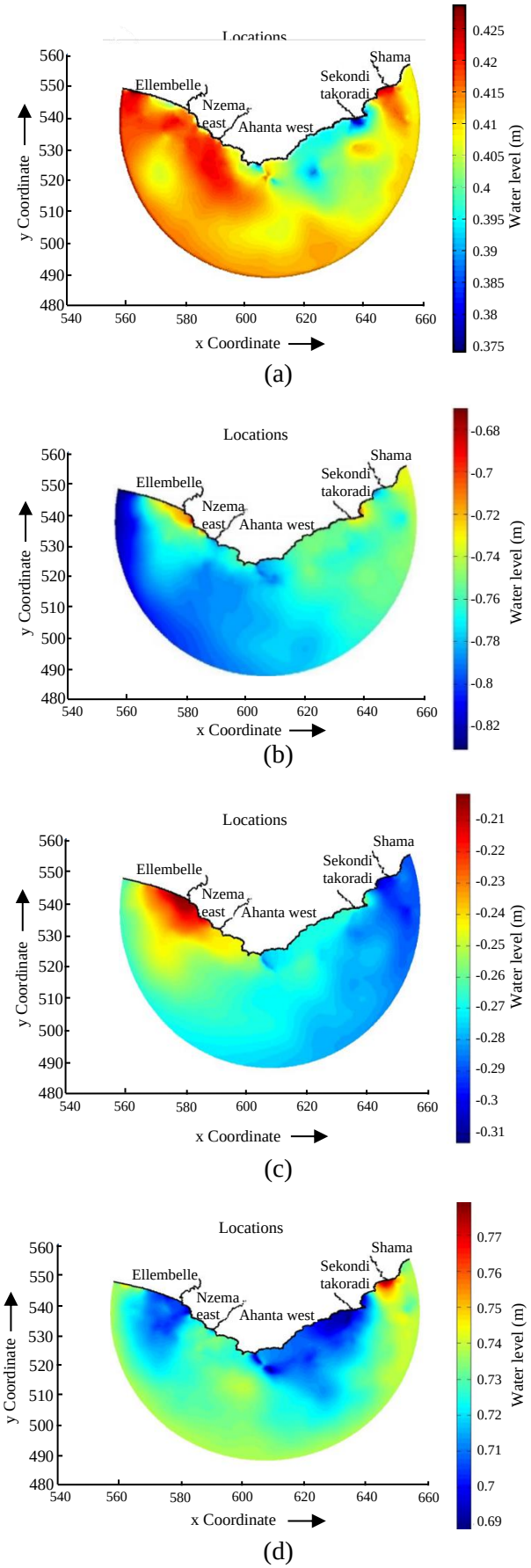

Fig. 4. Distribution of water level during neap tide and spring tide in the dry season (a-d).

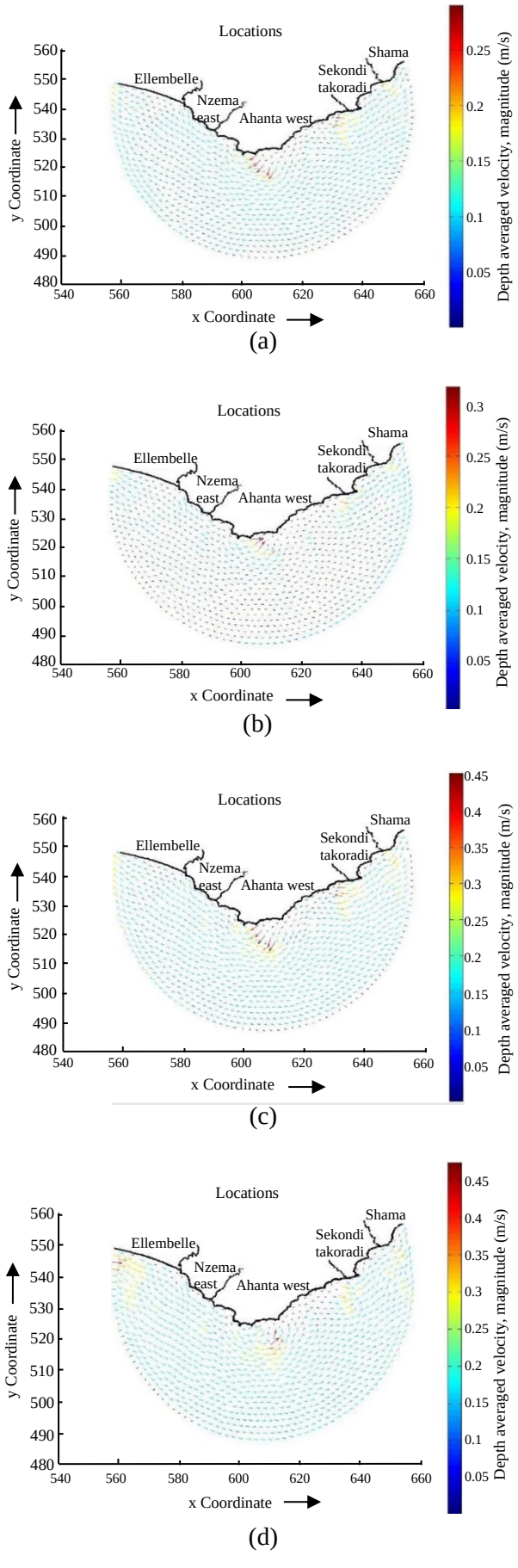

Fig. 5. Distribution of ocean velocity during neap tide and spring tide in the dry season (a-d).

The dynamics of ocean currents for each tidal condition during the dry season are presented in Fig. 5.

Red and orange represent the areas with higher velocities, while blue represents the areas with lower velocities. In Fig. 5(a), the ocean velocity ranges from roughly 0.05 m/s to 0.25 m/s during flood neap tide. In accordance with the flood phase of the tide, the water mostly flows inward toward the coast. Denser arrow concentrations are found in the vicinity of Shama and Sekondi Takoradi, suggesting that there are more tidal currents or flow in these places during the flood phase.

In Fig. 5(b), the water velocities vary from around 0.05 m/s to 0.3 m/s at ebb neap tide. In line with the ebb phase, the water flows away from the coast, symbolizing the water retreating or flowing out. The velocity range in Fig. 5(c) is 0.05 to 0.3 m/s at flood spring tide. In the direction of a flood tide, the direction is primarily landward. The way the water moves varies noticeably. Figure 5(d) shows the velocity range from 0.05 m/s to 0.45 m/s at ebb spring tide. An ebb tide is consistent with the direction of the water movement, which is away from the coast.

In general, ocean currents flowed towards the western area during flood tide, while reversed currents towards the eastern area occurred at ebb tide. The ocean water moved with velocities ranging from 0.05 to 0.35 $m.s^{-1}$ during neap tide. The current velocity was increased in the springtide with a range of 0.1 to 0.45 $m.s^{-1}$ in the model. It was caused by the higher tidal co-range during springtide instead of the neap tide. The ocean water flowed faster while either a peak of flood or ebb tide occurred. These velocity increases are relatively occurring in coastal waters, such as the Ahanta West Coast, Sekondi West Coast, and the Ellembelle West Coast. There was a decrease in the ocean velocities offshore.

Rainy season

The distribution of sea levels at the neap tide and spring tide during the rainy season is presented in Fig. 6.

Figure 6(a) water levels are roughly in the range of 0.36 and 0.41 meters. Most places in the region have comparatively higher water levels, particularly those around Ellembelle and Nzema East. Figure 6(b) illustrates the approximate range of the water level during ebb neap tide, which is -0.32 to -0.25m.

The water level range in Fig. 6(c) is roughly between 0.58 and 0.68 meters. The water level is highest at Ellembelle. From Ellembelle, the water level drops eastward toward Ahanta West. The lowest water levels are seen in the center area between Nzema East and Ahanta West. Figure 6(d) ebb tide water level ranges from roughly -0.89 to -0.68 meters. The deepest water level is found in the vicinity of Nzema East and Sekondi Takoradi. During ebb tide, the sections closest to Ellembelle have the lowest water levels.

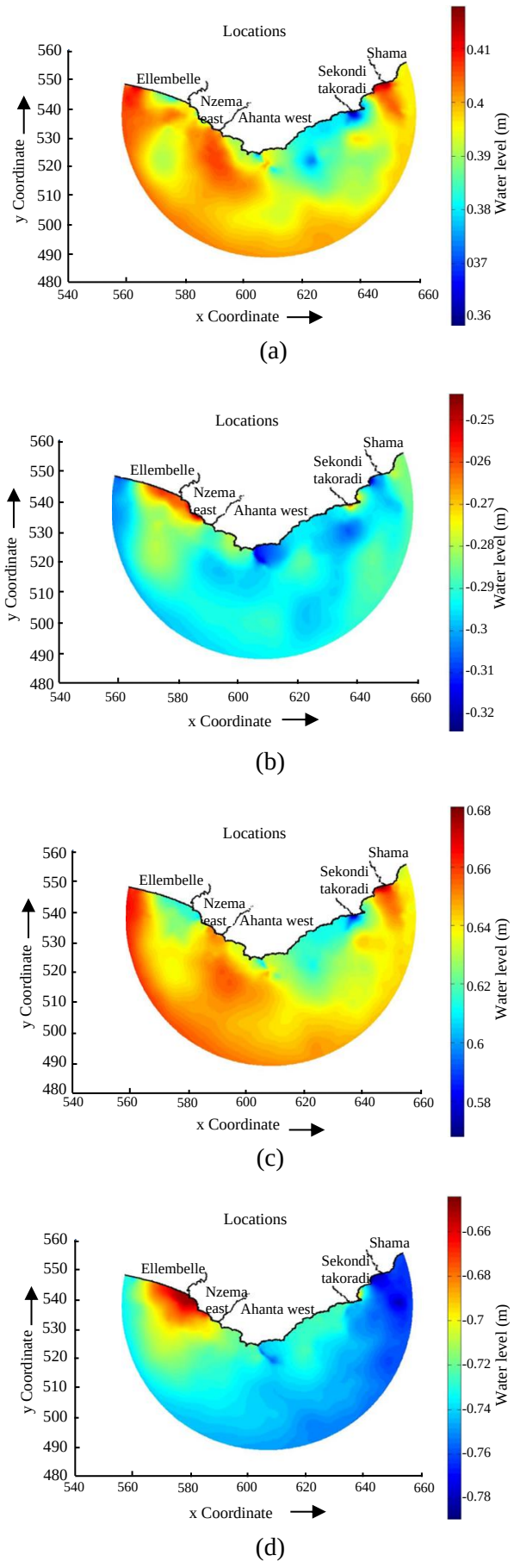

Fig. 6. Distribution of water level during neap tide and spring tide in the rainy season (a-d).

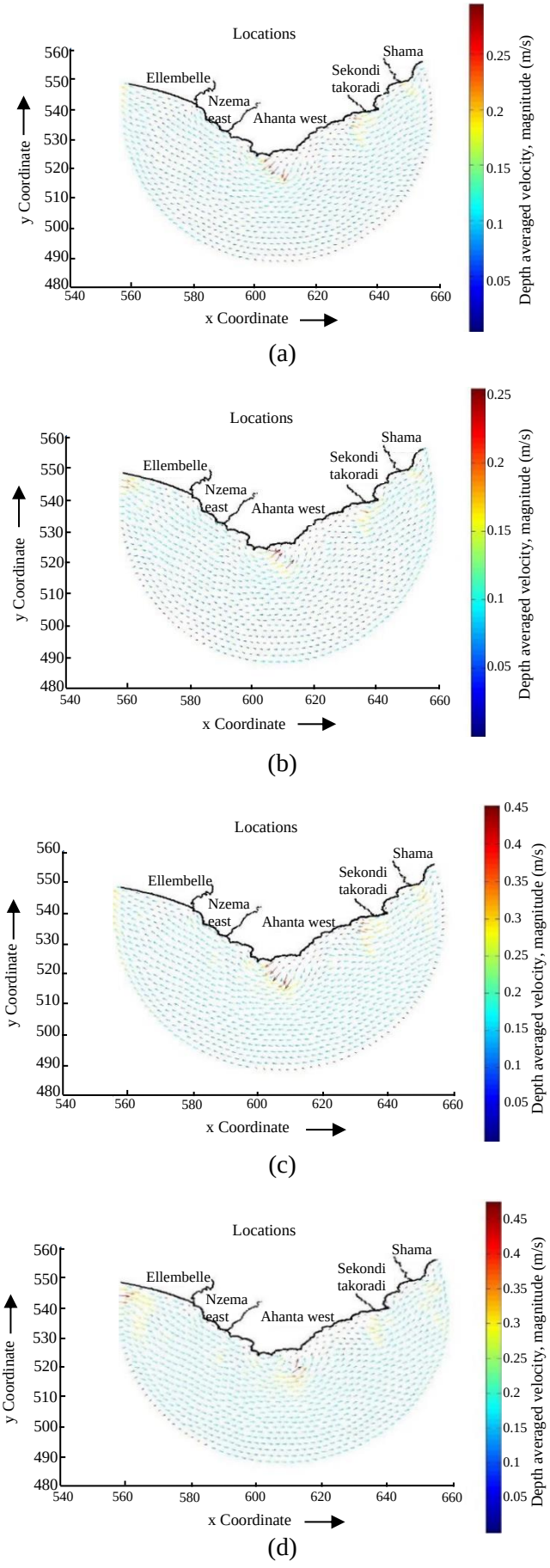

Fig. 7. Distribution of ocean velocity during neap tide and spring tide in the rainy season (a-d).

There was no significant difference in the tidal co-range between the rainy and dry seasons from the model. The tidal co-range was about 0.73 m for neap tide and 1.5 m for spring tide during the rainy season. The distribution of sea level height was also not significantly different between the dry season and the rainy season. It meant that rainfall did not influence the sea height dynamic largely in this area. The sea level rose as long as offshore at flood tide, while the sea level decreases as long as offshore at ebb tide.

The dynamics of ocean currents in the rainy season as shown in Fig. 7. were similar to that of the dry season. However, some ocean velocities showed lower values during the rainy season rather than the dry season in coastal waters.

In Fig. 7(a), the velocity ranges roughly from 0.05 to 0.25 m/s. Overall, the direction suggests that the water is moving landward, which is consistent with a flood tide. The range of ocean velocity in Fig. 7(b) is 0.05 to 0.25 m/s. The arrows indicate an outward or seaward movement of water, corresponding with an ebb tide, in contrast to the flood tide. The velocity in Fig. 7(c) varies between 0.05 and 0.45 m/s. The arrows primarily point towards the coast, signifying a flood tide (when water moves up towards the land).

In general, ocean velocities at ebb tide were increased rather than at flood tide. It indicated that the marine effluent will be relatively distributed towards the eastern area. Tidal force and surface wind are the dominant factors that affect the coastal dynamic. The tidal propagation did not show a significant difference between the rainy and dry seasons. Furthermore, in either rainy or dry seasons, the wind distribution tended to a low-level range, which is below 3 $m.s^{-1}$. Therefore, surface wind stress was considered unable to influence ocean dynamic changes between the dry and rainy seasons, although the wind direction of both seasons showed different patterns according to the model.

^{137}Cs radioactive waste dispersion

Emergency scenario in the rainy season

^{137}Cs dispersion model outputs for the emergency scenario during the rainy season are presented in Fig. 8 below.

As shown in Fig. 8(a), the dispersion is concentrated close to the release point. On the first day, the dispersion pattern is symmetrical, indicating little external influence. The dispersion area has greatly expanded on the seventh day, as seen in Fig. 8(b), with the ^{137}Cs extending outward from the initial point of release. Asymmetry in the dispersion pattern begins to emerge, suggesting the impact of atmospheric elements like wind. As seen in Fig. 8(c), on the 31st day following the release, the ^{137}Cs has dispersed over a vast area. A more distinct gradient in the dispersion shows that the concentration of ^{137}Cs is diluted with time and distance.

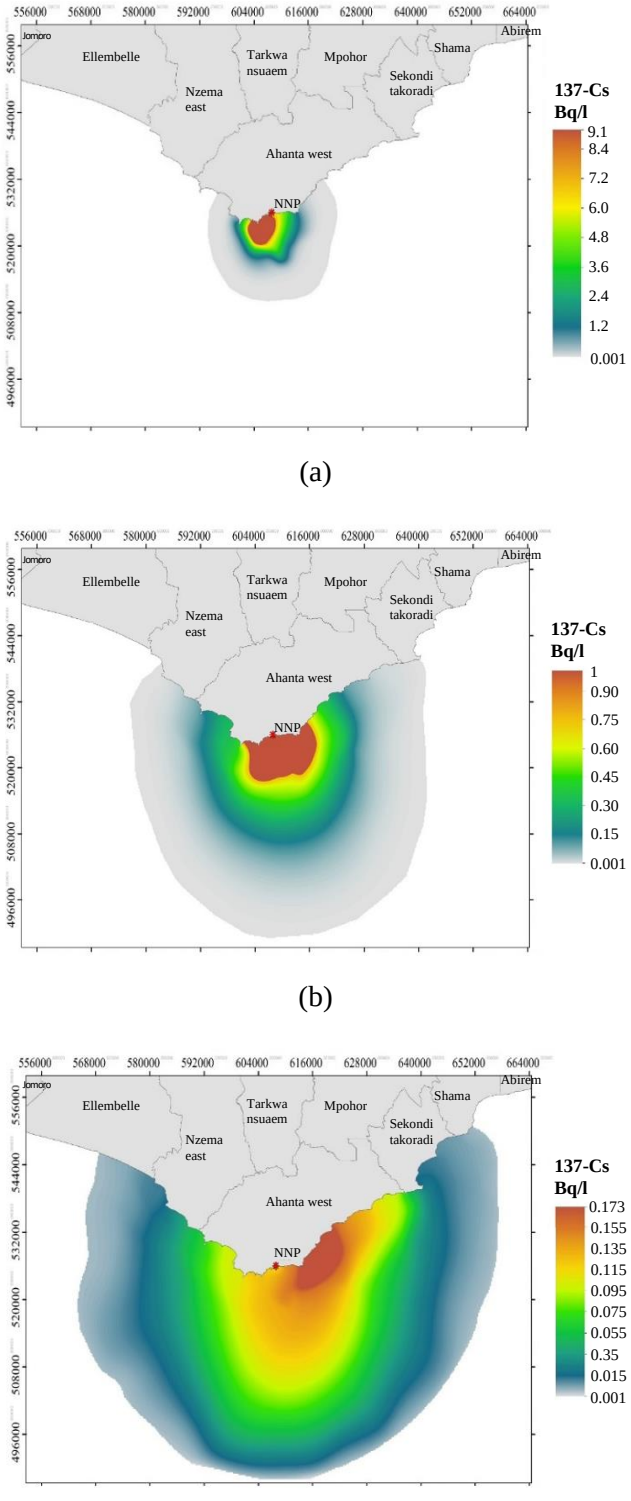

Fig. 8. Emergency Scenario of ^{137}Cs Dispersion in the rainy season (a-c).

The ^{137}Cs was still spreading around the Ahanta West waters within a radius of 16 km and the concentration was about 9.1 Bq.L^{-1}. There was a decrease in concentration from 9.1 Bq.L^{-1} to 1 Bq.L^{-1} after 1 week of effluent release. However, the dispersion of ^{137}Cs began moving in the opposite direction (eastern) as compared to the first distribution which was towards the west. The distribution of ^{137}Cs waste reached the entire coast of the Nzema East District on the 7th day. However high concentrations were still within the Ahanta West waters. This is illustrated in Fig. 8(b). The ^{137}Cs continued to spread into the eastern coast until the 31st day. The concentration range of ^{137}Cs had reduced to a level of about 0.173 Bq/L within the Ahanta West coastal waters on the 31st day after its release as shown in Fig. 8(c). There will be a continuous reduction in the levels of activities due to dispersion even after 31 days.

Emergency scenario in the dry season

^{137}Cs dispersion model outputs for the dry season are shown in Fig. 9.

Figure 9(a) illustrates the dispersion of 137Cs concentrated around the release site on the first day of the release. The ^{137}Cs are only slightly dispersed from the site of initial discharge. On the seventh day, as shown in Fig. 9(b), the dispersion grew farther away from the source. The dispersion's spread points to a potential wind pattern that may be affecting the movement. Figure 9(c) illustrates how ^{137}Cs have spread much more, taking up more space on the 31st day after the release. There has been an even greater fall in concentration close to the release site.

For the first day of release, the activity was around 9.1 Bq. L^{-1} and this waste was still dispersing. After a week of the release, the activity decreased from 9.1 Bq. L^{-1} to 1 Bq. L^{-1} Just as in the rainy season, there was a decrease in activity from 9.1 Bq. L^{-1} to 1 Bq. L^{-1} after 1 week of effluent release. However, as opposed to the initial distribution, which was westward, the radioactive Cs dispersion started traveling in the opposite direction (eastern) just as seen in the rainy season.

On the seventh day, the ^{137}Cs waste distribution had covered the whole shoreline of the Nzema East District. However, the Ahanta West waters still had significant activities. This is illustrated in Fig. 9(a). Up to the 31st day, the ^{137}Cs spread to the eastern coast. On the 31st day after its discharge, the ^{137}Cs concentration range had reduced to a level of about 0.166 Bq. L^{-1} at the Ahanta West waters.

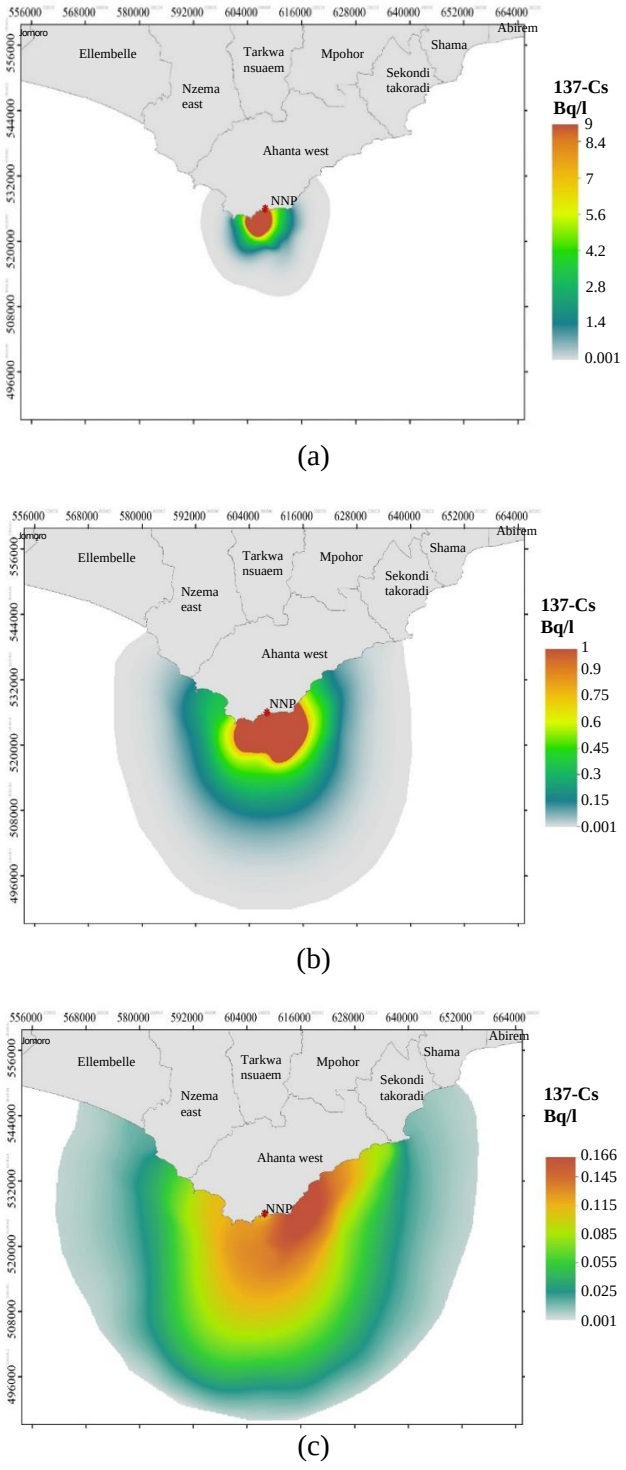

Fig. 9. Emergency scenario of ^{137}Cs Dispersion in the dry season (a-c).

^{137}Cs remain dissolved in the water column due to its geochemical nature thereby making it a conservative radionuclide. The conservative nature of ^{137}Cs causes its distribution to match the current movement trend [19]. The ocean current, which regulates the concentration of all pollutants in the marine environment, is responsible for the wide distribution and drop in ^{137}Cs concentration [20]. The ocean current in this area is mostly driven by

tides and winds. The type of current in this area is the Guinea current. The Guinea Current, a surface current, is an extension of the Equatorial Counter Current that flows primarily eastward and is constrained to a layer of 10 to 40 m in thickness along the Ghanaian coastline [18]. Surface currents aid in the dispersal of ^{137}Cs to regions with lower concentrations, resulting in an expansion of the ^{137}Cs distribution area over time. This expansion of the distribution area will be accompanied by a drop in the concentration of ^{137}Cs [21]. This is because radionuclides undergo advection and diffusion processes when they enter the sea. Radionuclides are carried away by the ocean current because of advection whereas the diffusion process causes the radionuclides to move to areas of lower concentration [22] The strength of the wind determines how the ocean current will flow and can also strengthen and weaken it. Strong wind causes ocean currents to be stronger and move faster. The wind direction determines the direction of the surface current [23]

There was not much difference between ^{137}Cs dispersion during the rainy and dry seasons. This indicates that during the release in an emergency, both seasons will have the same dispersion rate. This could be attributed to the fact that the wind pattern for both seasons in the southern part of Ghana where Ahanta West is located, does not change much. Ghana is strongly influenced by the West Africa Monsoon winds. The predominant wind in southern Ghana is the south-westerly wind which blows moist air from the Atlantic Ocean onto the continent [24].

CONCLUSION

The dispersion of ^{137}Cs was simulated for thirty days after its release into the marine environment. In an emergency scenario where releasing radioactive waste is controlled, most of the ^{137}Cs was concentrated within the area of release for the first seven days. However, Ahanta West coastal waters still had most of the ^{137}Cs activities with low levels of activities spreading to other coastal waters within the surrounding district. The bulk of contamination will remain at the point of release. The distribution of the radionuclide is in conformity with the direction of the surface ocean current. Due to the insignificant difference in the dry and rainy seasons in the study area, the dispersion of ^{137}Cs activities for both seasons was very similar.

Over a crucial one-month period, the study has shed important light on the early dispersion patterns of ^{137}Cs in the marine environment after a hypothetical nuclear emergency event at an AP1000 reactor. Our results clarify the primary dynamics affecting the distribution of ^{137}Cs and identify possible regions that could be affected in the short term following a nuclear emergency. Despite the fact that the AP1000 is a typical reactor type, many aspects of the nuclear incident such as the quantity of ^{137}Cs released and the circumstances surrounding it are generalised.

This raises even more questions; therefore, findings need to be considered in light of this speculative situation. Although there are certain uncertainties in our work, we have made great efforts to identify, measure, and, to the extent possible, reduce their impact. The findings offer insightful information on the possible dispersion patterns of ^{137}Cs in the case of a nuclear emergency in a marine environment, information that can help with response and preparation plans. They ought to be understood considering the assumptions and uncertainties surrounding them, though.

ACKNOWLEDGMENT

Special thanks to the Regional Centre for Energy and Environmental Sustainability (RCEES) of the University of Energy and Natural Resources (UENR) and the Radiation Protection Institute of the Ghana Atomic Energy Commission for their support during the research.

AUTHOR CONTRIBUTION

Yvette Agyiriba Aggrey, Mark Amo-Boateng, David Okoh Kpeglo, Muslim Muslim and Akhmad Tri Prasteyo equally contributed to the authorship of this article.

REFERENCES

1. H. D. Livingston and P. P. Povinec, Ocean Coastal Manage. **43** (2000) 689.
2. A. Aarkrog, Deep Sea Res. Part II **50** (2003) 2597.
3. Y. Inomata and M. Aoyama, Earth Syst. Sci. Data **15** (2023) 1969.
4. J. V. I. Batlle, T. Aono, J. E. Brown *et al.*, Sci. Total Environ. **487** (2014) 143.
5. R. Periáñez, F. Qiao, C. Zhao *et al.*, Mar. Pollut. Bull. **170** (2021) 112645.
6. K. O. Buesseler, Sci. **369** (2020) 621.
7. Anonymous, National Energy Transition Framework 2022-2070, Ghana Ministry of Energy, Accra (2022) 1.

8. W. L. Chen, C. Y. Pan, H. H. Huang *et al.*, J. Radioanal. Nucl. Chem. **329** (2021) 1345.
9. IAEA, Estimation of Global Inventories of Radioactive Waste and Other Radioactive Materials, IAEA-TECDOC-1591, Vienna (2008) 1.
10. Anonymous, Generic Design Assessment AP1000 Nuclear Power Plant Design by Westinghouse Electric Company LCC, Environment Agency, Bristol (2017) 1.
11. A. T. Prasetyo, M. Muslim and H. Suseno, J. Trop. Mar. **24** (2021) 291.
12. P. B. D. Bois, P., Laguionie, D. Boust *et al.*, J. Environ. Radioact. **114** (2012) 2.
13. J. Hou, Y. Kang, C. Hu *et al*., Int. J. Sediment Res. **35** (2020) 386.
14. U. J. Wisha, T. A. Tanto, W. S. Pranowo *et. al*., Reg. Stud. Mar. Sci. **18** (2018) 177.
15. Anonymous, Hydro-Morphodynamics, Deltares (2014) 710.
16. H. Kawamura, A. Furuno, T. Kobayashi *et al*., J. Environ. Radioact. **180** (2017) 36.
17. K. Sakuma, T. Nakanishi, M. Yoshimura *et al*., J. Environ. Radioact. **208-209** (2019) 106041.
18. Environmental Protection Agency, State of the Marine Environment Report for Ahanta West, Ellembelle, Jomoro and Nzema East Districts in the Western Region of Ghana, Ghana Environmental Protection Agency, Accra (2020) 1.
19. M. Machida, S. Yamada, A. Iwata *et al*., J. Nucl. Sci. Technol. **57** (2020) 939.
20. M. Hassanvand and Z. Mirnejad, Prog. Nucl. Energy **116** (2019) 115.
21. M. Muslim, F. I. Maulana, H. Suseno *et al*., Atom Indones. **48** (2022) 231.
22. M. Muslim, H. Suseno and S. Saodah, J. Mar. Sci. **21** (2016) 143. (in Indonesian)
23. Y. P. Octavia, M. I. Jumarang and Apriansyah, Prisma Fisika **6** (2018) 1. (in Indonesian)
24. C. McSweeney, M. New and G. Lizano, UNDP Climate Change Country Profiles, Ghana. University of Oxford (2020) 1.